CHEMICAL ENGINEERING TRANSACTIONS
VOL. 70, 2018
A publication of AIDIC
The Italian Association of Chemical Engineering
Online at www.aidic.it/cet
Guest Editors: Timothy G. Walmsley, Petar S. Varbanov, Rongxin Su, Jiří J. Klemeš

ISBN 978-88-95608-67-9; **ISSN** 2283-9216
DOI: 10.3303/CET1870341

CFD Simulation of Cross-Flow Filtration

Daniela B. Dzhonova-Atanasova*, Iren H. Tsibranska, Stela P. Paniovska

Institute of Chemical Engineering, Bulgarian Academy of Sciences, Acad. G. Bonchev Str. Bl. 103, 1113 Sofia, Bulgaria
d.dzhonova@gmail.com

The aim of the present work is to study the transfer processes in a cross-flow filtration cell, in order to determine the conditions for stable and efficient operation of a side-stream filtration module, integrated with a bioreactor. The current interest in membrane integrated bioreactors is connected with the pursuit of energy and cost efficiency in a wide area of industrial applications, including wastewater treatment, food industry, pharmaceutical industry, and fuel production. A numerical CFD model is employed, based on previous experience with experimental concentration of antioxidants, such as polyphenols and flavonoids from extracts of natural products by nanofiltration. The geometry under investigation is a 3D model of the experimental flat-sheet cell with tangential orientation of the feed inlet. The swirling turbulent flow in the feed channel is favourable for reducing the concentration polarization layer on the membrane surface and preventing fouling. The main factors, affecting the filtration process, are the shear stress distribution and the concentration profiles in the vicinity of the membrane surface. The CFD models of mass transfer in cross-flow nanofiltration are scarce and there are none for the reference experimental filtration cell. The present CFD simulation reveals the concentration distribution in the feed channel. It complements previous data for the flow pattern with new knowledge on the mass transfer there, directed to understanding and control of the concentration polarization phenomenon. The numerical study uses the tools of ANSYS Fluent R13, based on the finite volume method for solving the Reynolds-Averaged Navier-Stokes (RANS) equations. The obtained results are analysed in rapport with available experimental data.

1. Introduction

Membrane separation coupled with bioprocesses is a promising engineering solution for energy and cost effective wastewater treatment, bioethanol production, and production of valuable substances for pharmaceutical and food industry. Integration of processes is a logical step towards reduced equipment cost and energy consumption and shorter operation time. A review of modern applications of integrated membrane operation in agro-food production is presented in (Cassano and Drioly, 2014). The authors point out that the main factors influencing the economic viability of membrane integrated technologies are high initial operating costs and increasing occurrence of membrane fouling. They discuss the difficulty to control concentration polarization (CP) phenomenon and membrane fouling for membrane technologies, applied to vegetable oils, fruit juice processing, and obtaining extracts with biologically active compounds.

CP is a result of the solute rejection by the membrane and represents a boundary layer with increased solute concentration near the membrane surface, which hinders the transport of the solvent towards the membrane, reaching stationary conditions. Membrane fouling is the permanent deposition of macromolecules, particles, colloids, and possibly cells and microorganisms on the surface or in the pores of the membrane, which reduces drastically the permeate flux and may lead to impossibility for operation. Fouling issues are analysed by Stoller et al. (2017) in ultrafiltration (UF) and nanofiltration (NF) of aqueous solutions.

Prediction and control of flux decline through the membrane is a long investigated research area including experimental and theoretical work. CFD is a strong tool to study the processes in the filtration modules. It reveals the distribution of the flow parameters in the calculation domain, showing a detailed hydrodynamic picture. It calculates the shear stress at the membrane surface, which strongly affects the formation of concentration polarisation layer and membrane fouling. The mass transfer at the membrane surface is another important factor directly related to concentration polarization and effective membrane operation.

Please cite this article as: Dzhonova-Atanasova D.B., Tsibranska I.H., Paniovska S.P., 2018, Cfd simulation of cross-flow filtration , Chemical Engineering Transactions, 70, 2041-2046 DOI:10.3303/CET1870341

The flow pattern is easily calculated, assuming impermeable wall boundary conditions at the membrane. It is based on the circumstance that in NF or UF processes the permeate flux is smaller than the feed flowrate by several orders of magnitude. However, this approach does not calculate the mass transfer and the process of filtration. This is achieved only by coupling the hydrodynamic with the mass transfer model and gives possibility to study the formation of concentration polarisation layer and the membrane rejection of the solute. Only a few coupled numerical solutions have been found, such as the model, proposed for NF in a slit-type channel (Geraldes et al., 2001) and applied to NF and reverse osmosis (RO) in a spacer filled channel (Keir, 2012); the models of a polarization layer, during RO in a slit-type channel (Salcedo-Díaz et al., 2014) and in a roto-dynamic filtration system (Jogdand and Chaudhuri, 2015).
One simpler approach, employed in the present work, is to estimate the mass transfer coefficient from the relation of mass transfer to velocity field in the viscous sublayer near the wall, proposed by Reiss and Hanratty (1963) and widely employed in membrane studies by the electrochemical technique for measuring the shear rate at the membrane surface. The mass transfer and the shear stress distribution at the membrane surface are two main factors directly affecting concentration polarization and effective membrane operation. The aim of the present work is to estimate the mass transfer in a cross-flow filtration cell.

2. Numerical model

The present numerical simulation by the techniques of ANSYS Fluent R13 is based on the experimental set up and observations on the flux behaviour in cross-flow organic solvent nanofiltration (OSN). The simulated cross-flow cell is taken from a study on concentration of polyphenols and flavonoids from ethanolic extract of *Sideritis ssp*. (Mursalski tea) by OSN (Tsibranska and Tylkowski, 2013). The reference experimental setup comprised a METcell cross-flow system (Membrane Extraction Technology Ltd., UK) with four connected in series flat-sheet cells, each with a membrane area of $5.4 \cdot 10^{-3}$ m^2, a cell height h = 0.005 m, at a constant flowrate of $2 \cdot 10^{-5}$ m^3/s, and a transmembrane pressure of 20 bar. Figure 1a shows the geometry and the flow pathlines of the flat circular cell.

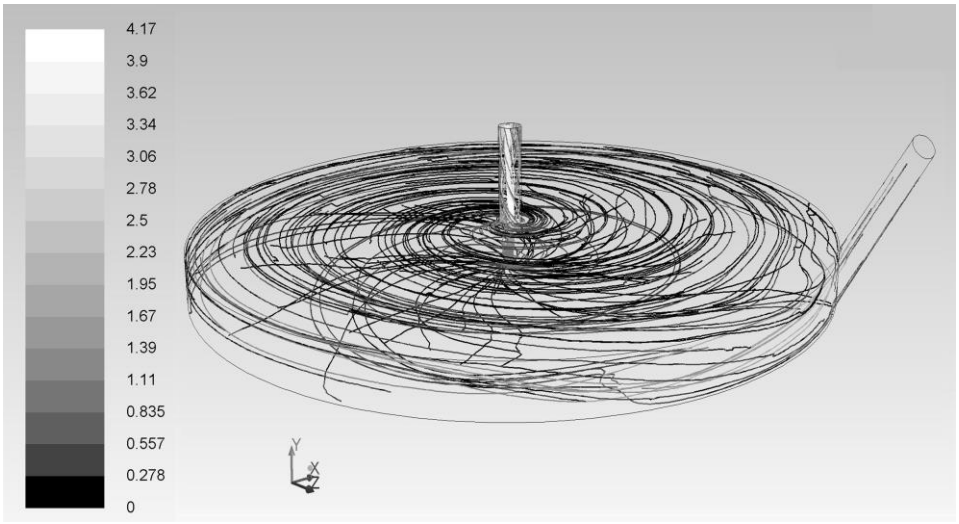

a

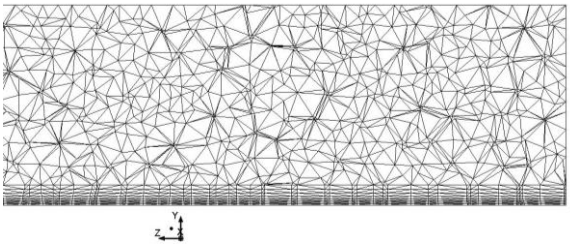

b

Figure 1: Flat-sheet cross-flow filtration cell. a) Pathlines coloured by velocity magnitude (m/s); b) Tetrahedral mesh with inflation at the membrane surface

The tangential feed inlet results in rotational turbulent flow in the cell, which ensures stable operation, by reducing concentration polarization and preventing from membrane fouling. The concentrate outlet is in the centre of the cell top. The cell bottom represents a membrane. Detailed scheme of the cell is given in (Peeva et al., 2004).
The transport processes in the cell are simulated as stationary by the RANS equations of continuity, momentum and species transport, closed by a realizable "k-ε" (RKE) model of turbulence (ANSYS Fluent R13.0, 2010).
The mesh of the 3D calculation domain is tetrahedral, allowing refinement near the surface of the membrane (Figure 1b). The mesh sizing of ca. 800,000 cells was found appropriate for mesh independent results.
The model liquid is Newtonian with constant physicochemical properties.
The following boundary conditions are specified: velocity inlet at the feed inlet; outflow at the concentrate outlet; no-slip conditions at the solid surfaces, including the membrane walls, where no-permeation and constant species concentration is assumed (dissolving wall).
The local and the average mass transfer coefficients at the membrane surface are targeted by the simulations compared to experimental data from the literature.
The local mass transfer coefficient k_L (m/s) is evaluated from the distribution of the wall shear stress on the membrane surface by using the correlation of Reiss and Hanratty (1963). It relates local shear rate and boundary layer diffusion rate via Eq(1):

$$k_L = 0.892 \left(\frac{\tau D^2}{\mu d_e}\right)^{1/3}, \quad (1)$$

where τ indicates the wall shear stress (Pa), μ stands for liquid dynamic molecular viscosity (0.001 kg/ms), D is the diffusion coefficient (~ $6.7 \cdot 10^{-10}$ m^2/s) and d_e is the sensor diameter (0.001 m) in the model system employed in (Vlaev et al., 2006).
The simulation uses hydrodynamic and concentration conditions typical for OSN. The feed flowrates reported in (Peeva et al., 2004) were in the range $1.17 \cdot 10^{-5}$–$4.17 \cdot 10^{-5}$ m^3/s and in (Tsibranska and Tylkowski, 2013) $2 \cdot 10^{-5}$ m^3/s. The feed concentration for nanofiltration varied in a wide range in literature sources. It reached up to 0.15 wt% total phenolic content in ethanol in (Tsibranska and Tylkowski, 2013) and up to 20 wt% docosane and TAOBr in toluene in (Peeva et al., 2004).
The present work obtains results for filtration at feed flowrates Q_f = $1.17 \cdot 10^{-5}$, $2 \cdot 10^{-5}$ and $4.17 \cdot 10^{-5}$ m^3/s. It assumes feed mass fraction of solute c_f = 0.01 kg/kg (1 wt%) and mass fraction of solute at the membrane c_{fm} = 1.5 c_f comparable to the values reported in (Peeva et al., 2004).

3. Results and discussion

At Q_f = $2 \cdot 10^{-5}$ m^3/s, Schmidt number $Sc = \mu/\rho D$ = $1.5 \cdot 10^3$ and constant properties of the solution, where ρ is liquid (mixture) density (kg/m^3), the local mass transfer coefficient at the membrane surface, calculated by Eq(1), is shown in Figure 2. The distribution seems quite regular, with the exception of small regions of high values at the periphery and the centre of the membrane, corresponding to high shear stress.
For the visualization of the concentration distribution and the concentration boundary layer, simulations are performed at Sc = 10 because the small dimensions of the concentration layer at the typical in filtration Schmidt number Sc ~ 10^3 need very fine mesh close to the membrane surface and much more computational time. The concentration boundary layer is about 1/10 of the viscous sublayer at typical conditions of cross-flow filtration (Reiss and Hanratty, 1963). Figures 3 and 4 illustrate the concentration boundary layer at the membrane surface. As seen in Figure 4a, the boundary layer thickness is smaller at higher velocity in the peripheral zone. In the case shown in Figure 4b of smaller Reynolds number (Re), due to higher viscosity, the boundary layer is much thicker and regular.
The space-average Sherwood number (Sh) is calculated by the correlation for turbulent flow in a pipe from Chilton-Colburn analogy (Chilton and Colburn, 1934):

$$Sh = 0.023\, Re^{0.8} Sc^{0.33}, \quad (2)$$

where $Sh = k_L' d_h / D$ and $Re = \rho v_f d_h / \mu$. Here k_L' denotes the average mass transfer coefficient (m/s), v_f is the feed inlet velocity (m/s), d_h indicates the flow hydraulic diameter (m).
In order to determine the hydraulic diameter, it is assumed that the fluid movement in the cell resembles flow in a spiral channel. Since the cell height h is much smaller than its diameter, the hydraulic diameter is calculated by $d_h = 2h$, which is accepted for large flow aspect ratio width to height.

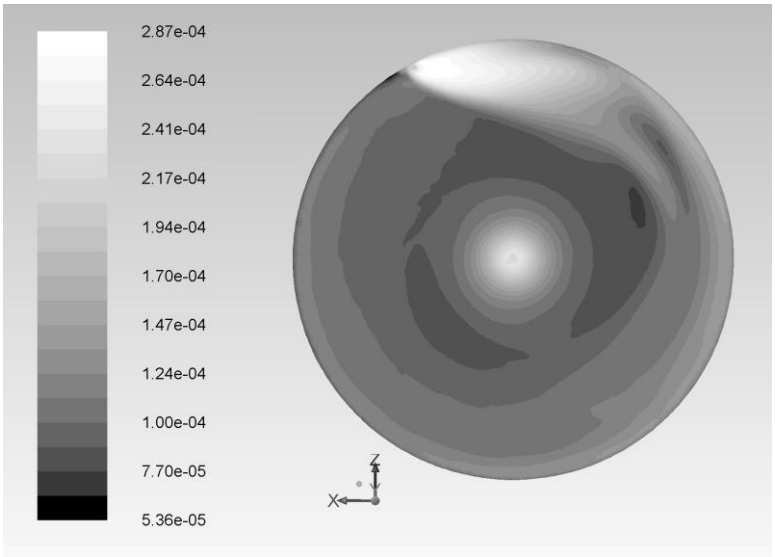

Figure 2: Contour plots of mass transfer coefficient distribution (m/s) on the membrane surface, $Q_f = 2 \cdot 10^{-5}$ m^3/s; Sc = 1,500; Re = 28,300

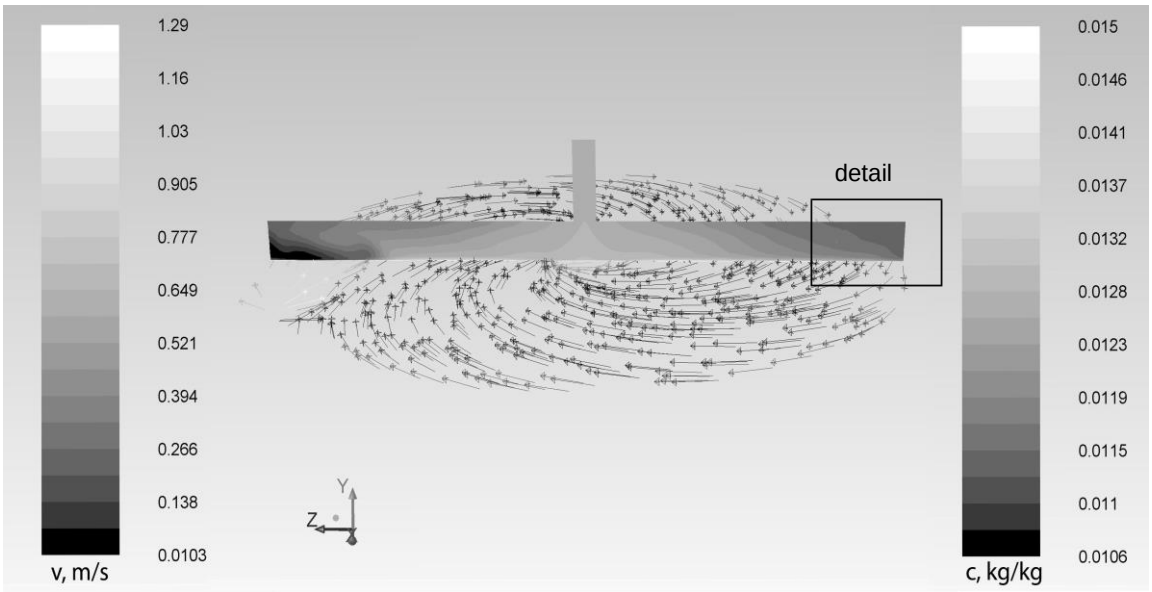

Figure 3: Contour plots of mass fraction c (kg/kg) at the mid-vessel plane, Sc = 10, $Q_f = 2 \cdot 10^{-5}$ m^3/s with velocity vectors in the vicinity of the membrane, coloured by velocity magnitude v (m/s)

The relation, Eq(2), is employed successfully in (Peeva et al., 2004) for OSN in a cross-flow cell with the same configuration, but larger membrane surface area ($7.8 \cdot 10^{-3}$ m^2). A comparison of our results for $k_L' = Sh\ D/d_h$ and *Sh* calculated by Eq(2) to reference data from literature sources is presented in Table 1. It can be seen that the values of the average mass transfer coefficient k_L' are comparable to the data of other authors. It should be noted that the lower values of the mass transfer coefficient, reported in (Peeva et al., 2004), are obtained for higher viscosity of the systems investigated there and bigger dimensions of the filtration cell, leading to lower cross-flow velocity. Table 1 shows a good agreement of the present results with the electrochemical measurements in (Koutsou and Karabelas, 2012) in a dead-end filtration cell with stirring.

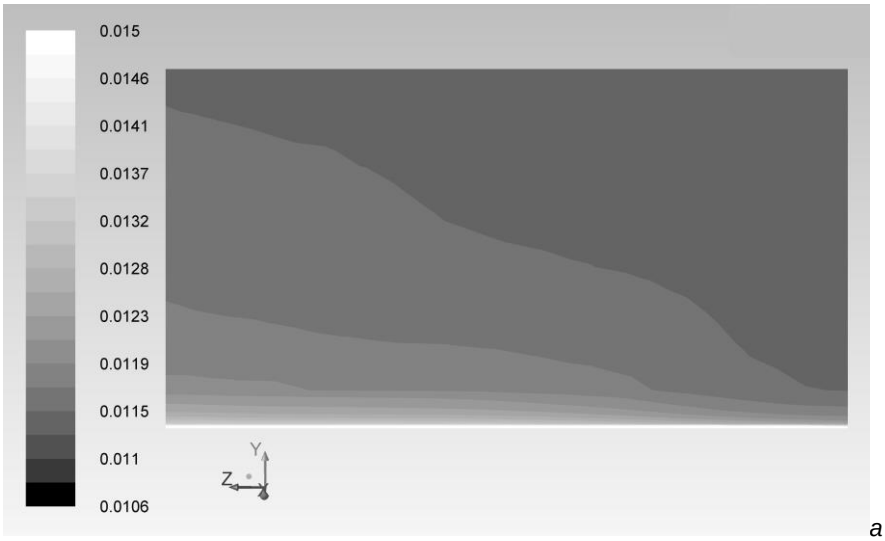

a

Sc = 10, Re = 28,300

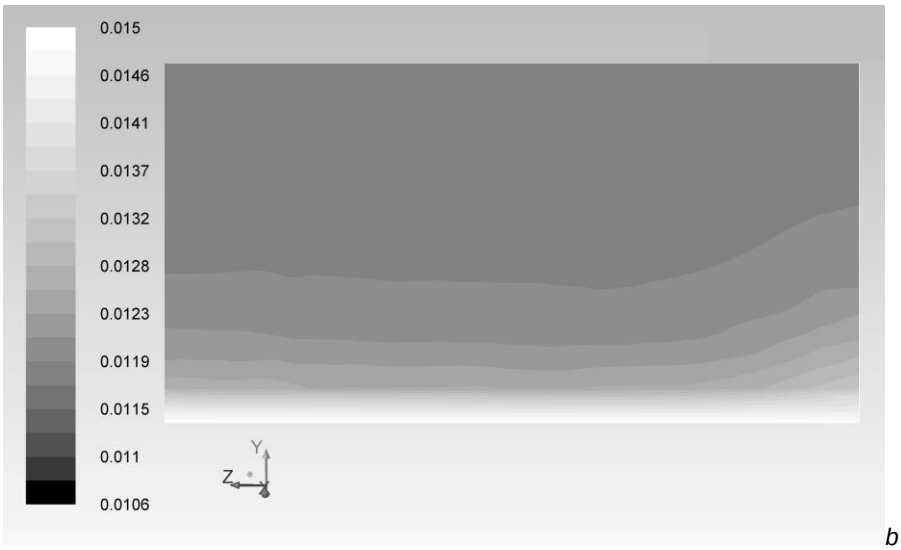

b

Sc = 10, Re = 2,830

Figure 4: Detailed view of contour plots of mass fraction (kg/kg) at the mid-vessel plane $Q_f = 2 \cdot 10^{-5}$ m^3/s; Sc = 10. a) Re = 28,300; b) Re = 2,830

Table 1: Comparison of calculated mass transfer coefficient with reference data

Author	$Q_f \cdot 10^5$ (m^3/s)	Inlet velocity v_f (m/s)	Volume-average cross-flow velocity v_{va} (m/s)	$Re \cdot 10^{-4}$	*Sh*	$k_L' \cdot 10^5$ (m/s)
This study, *Sc* = 1,500						
	1.17	1.58	0.57	1.58	586	3.93
	2	2.83	0.25	2.83	934	6.26
	4.17	5.90	1.70	5.90	1,680	11.3
Peeva et al. (2004)						
	1.17–2.17					0.6–1.9
	3.33–4.17					1.7–5.3
Koutsou and Karabelas (2012), *Sc* = 2,025						
					500–950	2–11

4. Conclusions

The calculated values of local and average mass transfer coefficients are comparable with the available reference data from literature sources. The picture of the local mass transfer coefficient obtained corresponds to the particular membrane shear stress distribution and is related to similar input parameters, such as cross-flow velocity and system physicochemical properties.
The tangential orientation of the feed inlet results in cell-contained swirling flow that sweeps the membrane surface and ensures tangential flow near the membrane, eliminating the need for in-built mobile components. The circular turbulent flow is favourable for high membrane shear stress, preventing fouling.
The increase in the mass transfer coefficient with cross-flow velocity, in agreement with experimental data, confirms the relation of the increase in the permeate flux with the reduction of the concentration polarization layer.
The method of mass transfer evaluation proposed allows assessment of the regimes in a side-stream cross-flow filtration cell for integrated processing.

Acknowledgments

The authors gratefully acknowledge the financial support of the National Science Fund of the Republic of Bulgaria, Contract DN 07/11/15.12.2016.

References

ANSYS Fluent R13.0, 2010, Theory Guide, Canonsburg, Pennsylvania, United States.
Cassano A., Drioly E. (Ed), 2014, Integrated membrane operations in the food production, De Gruyter, Berlin, Germany.
Chilton T.H., Colburn A.P., 1934, Industrial and Engineering Chemistry, 26 (11), 1183–1187.
Geraldes V., Semião V., De Pinho M.N., 2001, Flow and mass transfer modelling of nanofiltration, Journal of Membrane Science, 191, 109–128.
Jogdand A., Chaudhuri A., 2015, Modelling of concentration polarization and permeate flux variation in a roto-dynamic reverse osmosis filtration system, Desalination, 375, 54–70.
Keir G.P., 2012, Coupled modelling of hydrodynamics and mass transfer in membrane filtration, PhD thesis, Deakin University, Australia.
Koutsou Ch.P., Karabelas A.J., 2012, Shear stresses and mass transfer at the base of a stirred filtration cell and corresponding conditions in narrow channels with spacers, Journal of Membrane Science, 399–400, 60–72.
Peeva L.G., Gibbins E., Luthra S.S., White L.S., Stateva R.P., Livingston A.G., 2004, Effect of concentration polarisation and osmotic pressure on flux in organic solvent nanofiltration, Journal of Membrane Science, 236, 121–136.
Reiss L.P., Hanratty T.J., 1963, An experimental study of the unsteady nature of the viscous sublayer, AIChE Journal, 9 (2), 154–160.
Salcedo-Díaz R., García-Algado P., García-Rodríguez M., Fernández-Sempere J., Ruiz-Beviá F., 2014, Visualization and modelling of the polarization layer in cross-flow reverse osmosis in a slit-type channel, Journal of Membrane Science, 456, 21–30.
Stoller M., Pulido J., Di Palma L., 2017, Study on fouling behaviour of ultrafiltration and nanofiltration during purification of different organic matter polluted wastewaters, Chemical Engineering Transactions, 60, 296-299.
Tsibranska I.H, Tylkowski B., 2013, Concentration of ethanolic extracts from Sideritis ssp. L. by nanofiltration: Comparison of dead-end and cross-flow modes, Food and Bioproducts Processing, 91, 169–174.
Vlaev S.D., Nikov I., Martinov M., 2006, Shear and skin friction on particles in power-law fluids agitated by flat-blade and fluid foil impellers, Chemical Engineering Science, 61, 5455–5467.